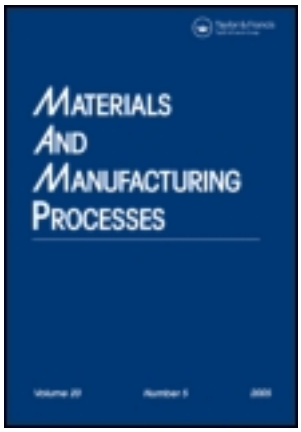

Materials and Manufacturing Processes
Publication details, including instructions for authors and subscription information:
http://www.tandfonline.com/loi/lmmp20

Deep Drawing of Aluminum Alloys Using a Novel Hydroforming Tooling

Faramarz Djavanroodi [a], D. Sharam Abbasnejad [a] & E. Hassan Nezami [a]
[a] Iran University of Science and Technology, Mechanical Engineering Department, Tehran, Iran

Available online: 10 May 2011

To cite this article: Faramarz Djavanroodi, D. Sharam Abbasnejad & E. Hassan Nezami (2011): Deep Drawing of Aluminum Alloys Using a Novel Hydroforming Tooling, Materials and Manufacturing Processes, 26:5, 796-801

To link to this article: http://dx.doi.org/10.1080/10426911003720722

Materials and Manufacturing Processes, 26: 796–801, 2011

ISSN: 1042-6914 print/1532-2475 online
DOI: 10.1080/10426911003720722

Taylor & Francis
Taylor & Francis Group

Deep Drawing of Aluminum Alloys Using a Novel Hydroforming Tooling

Faramarz Djavanroodi, D. Sharam Abbasnejad, and E. Hassan Nezami

Iran University of Science and Technology, Mechanical Engineering Department, Tehran, Iran

A simplified sheet hydroforming tooling was designed, fabricated, and tested. The advantage of the new tooling is its simplification of the tools, its requirement of lower hydraulic pressure for forming and decreasing the cost of the process. In this article, a new method of hydroforming deep drawing assisted by floating disk is proposed and investigated through experiments and simulation. Moreover, its advantages, such as simplifying the tools, decreasing the required medium pressure of the forming process, and elimination of some wrinkle due to ironing effect, have been discussed. An aluminum alloy, Al6061-T6, is formed successfully, and the influence of process parameters including the punch nose radius and friction are studied. It is determined that decreasing punch radii and friction, lead to a decrease in initial pressure and an increased safe zone, respectively. Working pressure curves, which guarantee sound workpieces, have been founded by series of experimental results. Wrinkling and fracture modes are studied and predicted in experiment and simulation. The finite element (FE) analysis is carried out. Hill–Swift and North American Deep Drawing Research Group (NADDRG) theoretical forming limit diagram (FLD) models are used to specify fracture initiation in finite element model (FEM), and it is shown that Hill–Swift model gives a better prediction. The simulated results are in good agreement with the experiment.

Keywords Al6061-T6; Design; Failure; Hydroforming; Sheet.

Introduction

Hydroforming has been one of the fundamental sheet metal forming processes for quite along time. The female die in the conventional deep drawing process is replaced by hydromechanical deep drawing process by a counter pressure created from a fluid. A rubber diaphragm prevents leakage and a punch determines the final shape of the workpiece. The fluid pressure acts as blank holder and prevents wrinkles [1].

Following the development of the relevant technologies, such as equipment design and manufacturing, automatic control systems, ultrapressure units, etc. many different methods have been invented. Hydroforming can be applied successfully in large volume production. It is believed that the future of the hydroforming still remains quite exciting and prospective. Many materials can be used in this process, such as low carbon steel, stainless steel, high strength steel, aluminum alloy, magnesium alloy, titanium alloy, etc. Actually, almost all of the materials used in conventional stamping can be used in sheet hydroforming. Depending on the different means, the liquid pressure in the die cavity is from around 30 to 150 MPa, but the usage of 200 MPa has also been reported [2]. Advantages and disadvantages of minus pre-bulging (MPB) and plus pre-bulging (PPB), and failure modes of hydrodynamic deep drawing were investigated by Lang et al. [3].

Compared with the conventional deep drawing process, the limit drawing ratio can be increased from 1.8 to 2.8, the tool costs can be reduced remarkably as only one tool half (the punch) is used. The female die is replaced with the chamber fluid; only the punch needs to be varied when drawing parts with different shapes and dimensions [3–6].

The quality of the formed parts can be influenced by the material properties. Anisotropy has more influence on the parts shape and the thickness distribution than in the conventional deep drawing process as the drawing ratio in the hydroforming deep drawing (HDD) process is usually very high [7].

Shim et al. [8] have introduced, a simple method to determine optimal pressure curve for the sheet hydroforming process. This process can be studied and developed systemically by using numerical simulation; the work will be helpful for practical industrial applications, especially for metal forming, and add to the knowledge base for "Virtual Design" or "Virtual Prototyping," which are both based on the FEM [9–11].

In this paper, a new method that combines hydrodynamic deep drawing and viscose pressure forming is introduced, and typical failure modes are studied. To determine wrinkling modes, Kawka et al. [12] have shown a numerical model, but they have mentioned that since several parameters can affect results of wrinkling simulation, maybe the FEM method can never estimate the wrinkling modes exactly. In addition, this paper emphasizes the use of numerical simulation to analyze the deformation process of the blank and provides the effective methods to prevent failures during the process. Failure limit diagrams (FLD) like the North American Deep Drawing Research Group (NADDRG) model [13] and the Hill–Swift model [14] were chosen to predict fracture initiation and compared with each other The Al6061-T6 aluminum alloys were used in the investigation.

Received July 24, 2009; Accepted January 29, 2010
Address correspondence to F. Djavanroodi, Iran University of Science and Technology, Mechanical Engineering Department, Tehran 16846-13114, Iran; E-mail: f.roodi@ic.ac.uk

Hydroforming test

In addition to the methods mentioned previously in this paper, hydroforming assisted by a floating disk is a new method that can simplify the tools used for hydroforming and decrease the cost of the process. With a floating disk, two sides of a blank will suffer equal friction force due to the normal blank holding force, in contrast to hydrodynamic deep drawing and viscose pressure forming processes, in which the medium in the chamber is in contact with one side of the blank. Therefore, the normal blank holding force and chamber pressure will be almost halved, and the punch force can consequently be decreased. Moreover, the needed equipments can be very simple and inexpensive, because the need for an independent hydraulic system to control the blank holding force and a complicated control system to adjust the gap between the die and blank holder can be avoided; thus, the cost of the die and the hydraulic press will be decreased.

The plus pre-bulging (PPB) function is applied to increase the formability of sheets in the hydroforming of Al6061-T6 [3].

Materials

The material used in this work is an Al–Mg–Si aluminum alloy, AL6061-T6, with a thickness of 0.8 mm. The reason for selecting the Al6061 is the wide use of this alloy in the Aerospace industry. Table 1 displays the properties of the material obtained from a uniaxial tensile test based on ASTM E.8 and ASTM E.517.

Tools

The essential tools include a punch, a blank holder, a pressure chamber, a rubber diaphragm, and a floating disk, as shown in (Fig. 1). The diaphragm at the bottom can move up and down due to the pressure of the viscous medium in the chamber; therefore, it makes the disk move up and down. The blank is placed between the blank holder and the floating disk. The blank holding force (BHF) due to the pressure of the chamber and the area of the floating disk can press the blank tightly to the blank holder. As the punch moves down, forming a cup, a control valve regulates the liquid flow, and the blank holding force can consequently be controlled. The pressure curve for successful forming was approximated theoretically beforehand and corrected experimentally.

Table 1.—Properties of the material Al6061-T6.

	Rolling direction		
Parameters	0°	45°	90°
Density (kg/m^3)	2700	2700	2700
Yielding stress (Mpa)	305	302	300
Ultimate tensile stress (Mpa)	346	342	341
Strain hardening exponent (n)	0.17	0.18	0.16
Hardening coefficient, k (Mpa)	570	550	549
Total elongation (%)	19	19	18
Poisson's ratio (ν)	0.33	0.33	0.33
Anisotropy factor (r)	0.48	0.7	0.53
Thickness (mm)	0.8	0.8	0.8

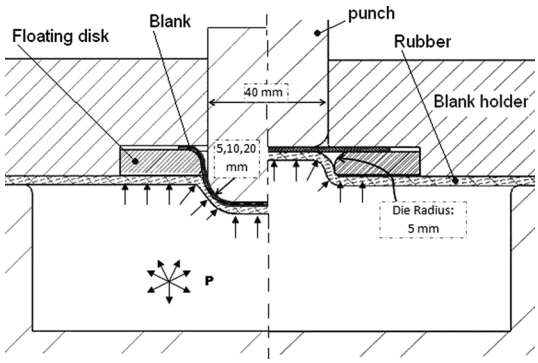

Figure 1.—The hydroforming process assisted by a floating disk.

All of the experiments were carried out using a 250-ton hydraulic double-action press. Figure 2 shows the equipment used, and Table 2 gives the dimensions of the tools used for this process.

Procedure

A rubber diaphragm is used to separate the fluid and the floating disk as well as the blank. The blank is then placed between disk and blank holder and centered. The blank holder is then placed on top and fastened. Pressure in the cavity is gradually raised to form the blank upward in reverse direction (PPB). The rigid punch moves down into fluid chamber, and the blank is forced to assume the shape of the punch. A pressure relief valve is used to regulate the fluid pressure in the chamber.

Results and discussion

Punch Radii Effects

Figures 3 and 4 show the chamber pressure and punch force vs. the punch stroke, respectively, for different punch

Figure 2.—Hydraulic press.

Table 2.—Tool dimensions.

Parameters	Values
Punch diameter d (mm)	40
Inside die(disk)diameter d_d (mm)	43.5
Punch nose radius r_p (mm)	5, 10, 20
Die entrance radius r_{die} (mm)	5
Inside blank holder diameter d_c (mm)	40.2
Blank holder entrance radius R_c (mm)	2

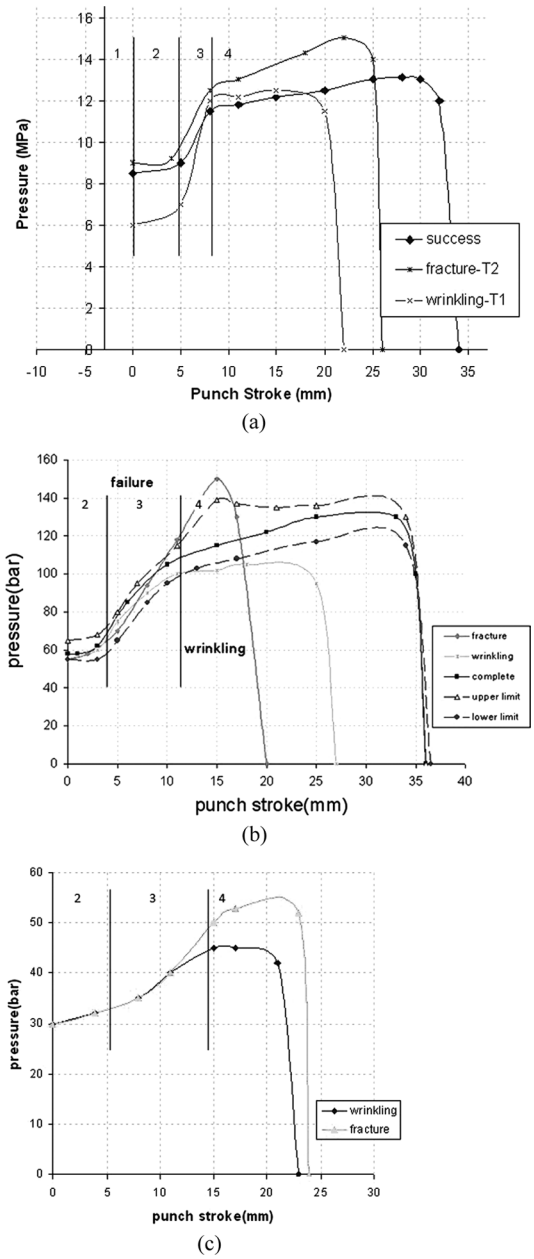

FIGURE 3.—Pressure-punch stroke curves for Al6061-T6 with LDR = 2: (a) punch radius = 5; (b) punch radius = 10; and (c) punch radius = 20.

nose radii. The punch's nose radii were 20, 10, and 5 mm. Equations (1) and (2) were used to obtain the approximate minimum and maximum limits of the initial pressure [7]. Equation (1) is the punch force that causes shearing of the blank, and Eq. (2) is the blank holding force by the fluid pressure acting on a flange area, e.g., the die contacting area

$$F_{\text{punch}} = \pi \cdot d \cdot t \frac{\sigma_y}{\sqrt{3}} \tag{1}$$

$$F_{\text{flange}} = \frac{\pi}{4}(D'^2 - d'^2) \cdot p_{\text{req}}, \tag{2}$$

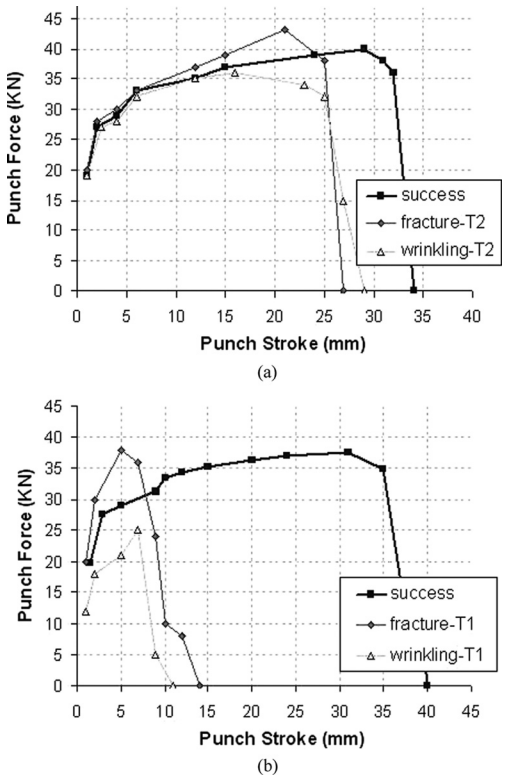

FIGURE 4.—Punch force-punch stroke curve for Al6061-T6 with LDR = 2: (a) punch radius = 5 and (b) punch radius = 10.

where D' is the blank diameter, d is the diameter of the blank contact region with the punch at the initial stage, d' is the inside diameter of the disk, t is the blank thickness, σ_y is the tensile yield stress of the blank material, and p_{req} is the required initial pressure. If the suppressing force due to fluid pressure is less than the punch force, then the blank tends to lift up. The suppressing force due to the fluid pressure should be higher than the punch force for a stable start of the process,

$$F_{\text{flange}} > F_{\text{punch}}. \tag{3}$$

Now, the minimum required initial pressure becomes

$$p_{\text{req}} = \beta \frac{4d \cdot t \cdot \sigma_y}{(D' - d'2)\sqrt{3}} \tag{4}$$

where p_{req} is the initial pressure setting and β is the correction factor to compensate for forming difficulty due to the shape of the cross-section: for a circular section, $1 \leq \beta \leq 2$ [7].

The calculated p_{req} for Al6061-T6 was 5.1 MPa, and by choosing $\beta = 1.2$, the initial pressure of the chamber becomes 6.1 MPa, which is in the safe zone relative to the experimental diagram for punch radius = 10.

Pressure in the die cavity can be divided into the following four zones [Fig. 3(a)]:

TABLE 3.—Friction coefficients between the surfaces.

Surfaces	SAE90 oil	Common grease	Orapi705 grease
Blank vs. Blank holder	0.1	0.06	0.01
Blank vs. Floating disk	0.1	0.06	0.01
Blank vs. Punch	0.13	0.13	0.13

1.) Zone 1 is pre-bulging, where the blank will be bulged 3 mm in the reverse direction;
2.) Zone 2 is the important stage where the initial pressure is applied, parameters can be calculated theoretically as mentioned before;
3.) Zone 3 is where the pressure increases with a sharp slope in comparison with the other zones;
4.) Zone 4 is the control zone.

Finally, the liquid pressure decreases rapidly and is released because the entire flange has been pulled into the die cavity. Decreasing punch radius leads to an increase of initial pressure needed (Fig. 3). However, in the other zones, the diagrams remain approximately the same. And a safe zone can be seen in which forming can be successfully performed [Figs. 3(a) and (b)]. On the other hand as the punch radius increases (20 mm), the safe zone is eliminated, and no successful forming can be performed, as show in Fig. 3(c). Reduction or increase of initial pressure would lead to wrinkle and fracture, respectively, and there will be no safe zone. This indicates that using a bigger punch radius would lead to a lower LDR.

Lubrication Effect

With a floating disk, two sides of a blank will suffer equal friction force due to the normal blank holding force, to determine the friction effect in this process; three types of lubricant were used, i.e., common SAE90oil, common grease, and special Orapi705grease, which can decrease the friction coefficient to 0.01. Friction coefficients between the surfaces based on the coulomb rule are shown in Table 3. Figure 5 shows the chamber pressure vs. punch force for different lubricant, as expected, good lubricant increases the size of the safe zone. With SAE90 oil, the process failed at the first stage while forming a specimen with LDR = 2; thus, using better lubricant was unavoidable. All experiments were done using common grease except those used to determine the effects of friction.

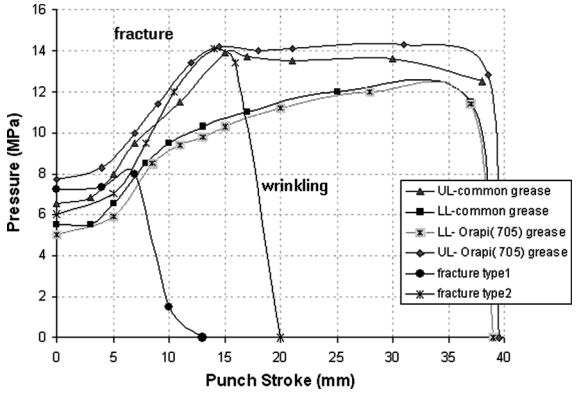

FIGURE 5.—The effect of using a good lubricant while forming Al6061-T6.

FEM Analysis

Explicit FE code was used to simulate the process. Because of the symmetric character of the forming, only a quarter of the model was used. All tools were modeled using an analytical rigid, and the materials were modeled using S4R (a 4-node quadrilateral in-plane general-purpose shell with reduced integration; this will reduce the time of the process by eliminating some unnecessary integrated points) elements for fracture prediction and C3D8R (an 8-node linear brick with reduced integration) elements for modeling anisotropic effects in sheets. The mesh size was 0.55 mm and penalty contact interfaces were used to enforce the intermittent contact and the sliding boundary condition between the blank and the tool elements. The material parameters used for the blank were derived from the uniaxial tensile test (Table 1). Anisotropy options were calculated according to ASTM-E517, and r_0, r_{45}, and r_{90} were used to calculate F, G, H, N, L, and M, which are material constants in the Hill48 yield function.

Hill's potential function is an extension of the Mises function and can be expressed as

$$f(\sigma) = \sqrt{\begin{aligned} &F(\sigma_{22}-\sigma_{33})^2 + G(\sigma_{33}-\sigma_{11})^2 \\ &+ H(\sigma_{11}-\sigma_{22})^2 + 2L\sigma_{23}^2 + 2M\sigma_{31}^2 + 2L\sigma_{12}^2 \end{aligned}}, \tag{5}$$

where σ_{ij} denotes the stress components. The material constants can be expressed in terms of the six yield stress ratios, R_{11}, R_{22}, R_{33}, R_{12}, R_{13}, and R_{23}, according to Eq. (6).

In sheet metal forming, anisotropic material data is commonly defined in terms of the ratio of the width strain to the thickness strain. The stress ratios can then be defined as in Eq. (7). These calculated ratios were introduced into the FE software directly to simulate anisotropic material based on the Hill criteria:

$$\begin{aligned} F &= \frac{1}{2}\left(\frac{1}{R_{22}^2} + \frac{1}{R_{33}^2} - \frac{1}{R_{11}^2}\right), \\ G &= \frac{1}{2}\left(\frac{1}{R_{11}^2} + \frac{1}{R_{33}^2} - \frac{1}{R_{22}^2}\right), \\ H &= \frac{1}{2}\left(\frac{1}{R_{11}^2} + \frac{1}{R_{22}^2} - \frac{1}{R_{33}^2}\right), \\ L &= \frac{3}{2R_{23}^2}, \quad M = \frac{3}{2R_{13}^2}, \quad N = \frac{3}{2R_{12}^2} \end{aligned} \tag{6}$$

$$\begin{aligned} &R_{11} = R_{13} = R_{23} = 1, \quad R_{22} = \sqrt{\frac{r_{90}(r_0+1)}{r_0(r_{90}+1)}}, \\ &R_{33} = \sqrt{\frac{r_{90}(r_0+1)}{r_{90}+r_0}}, \quad R_{12} = \sqrt{\frac{3r_{90}(r_0+1)}{(2r_{45}+1)(r_{90}+r_0)}} \end{aligned} \tag{7}$$

To determine the location of the fracture in the FEM model, FLD data were applied to software indirectly based on the NADDRG, and Hill–Swift models by a user subroutine.

To simplify the experimental and theoretical determination of the FLD and utilize the FLD more easily in the press workshop, the NADDRG introduced an empirical equation [10]. According to this model, the FLD is composed of two lines through the point Fld_o in the plane-strain state. The slope of the lines located on the left and right sides of FLD are about 45^o and 20^o. The equation is

$$Fld_o = \frac{(23.3 + 14.13t_0)\, n}{0.21} \tag{8}$$

It has been proven that a good simulation of the forming limit strains can be given on the basis of Swift diffuse instability theory and Hill localized instability theory, where Swift's and Hill's theories are used to calculate the forming limit strains on the left and the right sides, respectively, of the FLD [10]. According to Swift and Hill's criteria, the formula for calculating the forming-limit strains can be written as follows, with $\alpha = \sigma_2/\sigma_1$:

For $\varepsilon_2 < 0$:

$$\varepsilon_{j1} = \frac{1 + (1-\alpha)r}{1+\alpha} n \tag{9}$$

$$\varepsilon_{j2} = \frac{\alpha - (1-\alpha)r}{1+\alpha} n \tag{10}$$

For $\varepsilon_2 > 0$:

$$\varepsilon_{f1} = \frac{[1 + r(1-\alpha)].[1 - \frac{2r}{1+r}\alpha + \alpha^2]}{(1+\alpha)(1+r).[1 - \frac{1+4r+2r^2}{(1+r)^2}\alpha + \alpha^2]}.n \tag{11}$$

$$\varepsilon_{f1} = \frac{[(1+r)\alpha - r].[1 - \frac{2r}{1+r}\alpha + \alpha^2]}{(1+\alpha)(1+r).[1 - \frac{1+4r+2r^2}{(1+r)^2}\alpha + \alpha^2]}.n \tag{12}$$

In general, the failure modes can be divided into two types: wrinkling and fracture. There were three kinds of wrinkling and three types of fracture modes in forming the sheet. Figure 6(a) shows three kinds of wrinkling in Al6061-T6. There are a number of reasons for wrinkling: die entrance radius is too large, the oil pressure is not enough, too small blank holder pressure (i.e., oil pressure is not enough), and lubrication. One would expect less wrinkling because of rigidity of floating disk and its ironing effects. The three modes of wrinkling are based on the zone in which wrinkling is happening, i.e., wrinkling in the first stage of the forming (zone 2), called initial wrinkling. The middle and final wrinkling will happen in the 3rd and 4th zone, respectively. Figure 6(b) shows the prediction of these failure modes by the simulation.

In the experiment, fracture can be divided into three types, as shown in Fig. 7: the initial fracture, the middle fracture, and final fracture. The initial fracture means that the forming process is interrupted because of fracture at the initial stage;

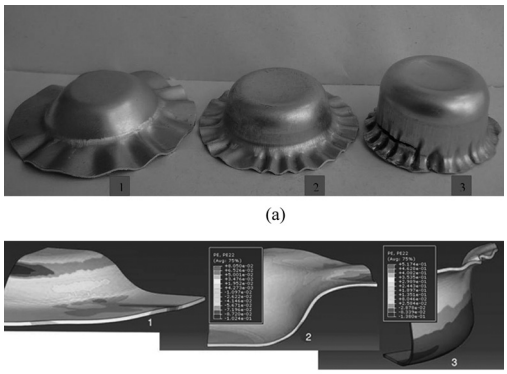

FIGURE 6.—Three types of wrinkling in Al6061-T6: (a) experimental and (b) simulation.

FIGURE 7.—Fracture modes in Al6061-T6.

this is caused mainly by insufficient initial liquid pressure, poor lubrication, and too large drawing ratio. The middle fracture emerges, when both the total punch force and the sheet drawing force reach the maximum. Good lubricant can prevent middle fracture mode. The final fracture mode arises because of the too large bending and unbending effects at the floating disk. Decreasing the liquid pressure at the final stage, use of a good lubricant on the flange prevents final fracture. Figure 8 presents the fracture modes, type one and type two, predicted by the FEM simulation. As can be seen

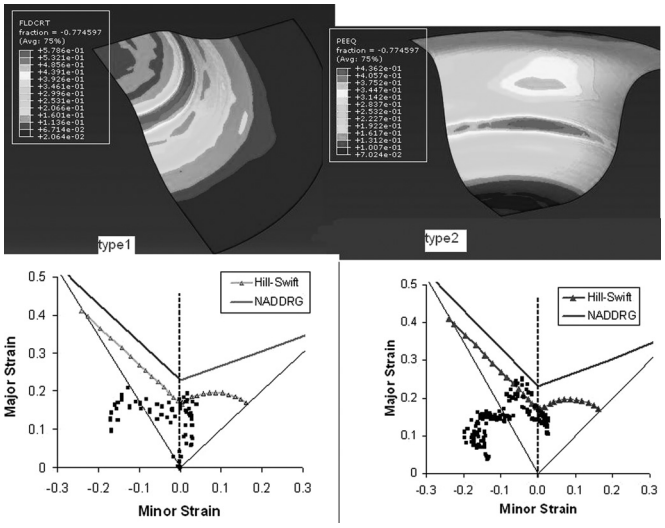

FIGURE 8.—Simulated fracture modes in Al6061-T6 with two FLD curves.

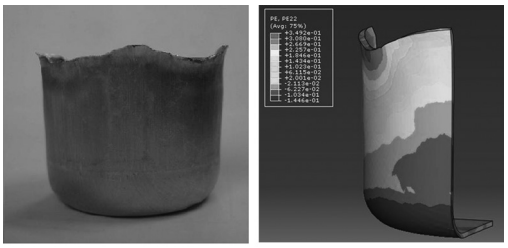

(a) (b)

FIGURE 9.—Successfully drawn Al6061-T6 with punch radius = 5: (a) experimental and (b) simulation.

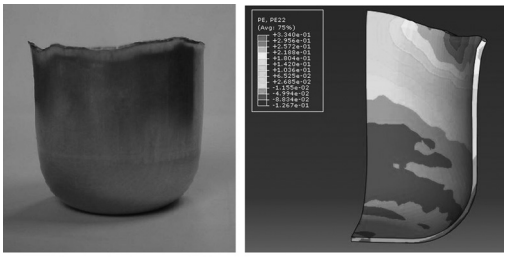

(a) (b)

FIGURE 10.—Successfully drawn Al6061-T6 with punch radius = 10: (a) experimental and (b) simulation.

in these figures, the FEM predicted both the wrinkling and fracture modes in this process; therefore, costly experiments can be avoided using a suitable FEM model.

Comparing the two FLD diagrams in Fig. 8, the Hill–Swift solution predicts the failure better than the NADDRG model; therefore, in the formation of this aluminum sheets, use of the former model is suggested. A good agreement has been obtained between experimental and simulated model for 5 mm and 10 mm dies radius as shown in Figs. 9 and 10.

CONCLUSION

A new method for hydroforming was proposed, and its advantages including decreases in chamber pressure, punch force, and cost of the process due to simplification of the tools and processes, were discussed. By using aluminum alloy, Al6016-T6, this new process was explored and studied, and good results were obtained.

1. Based on the deformation characteristics of this material, wrinkling and fracture modes are divided into three types as shown.
2. It was shown that increasing the punch radius leads to a decrease in the initial pressure, and consequently a decrease in the punch force in the second zone.
3. Decreases in the friction coefficient (using good lubricants) between the blank and floating disk leads to an increase in the size of the safe zone.
4. Finally, the results from both the simulation and the experiment are compared and proved to meet each other very well. The simulation is a very helpful method for analysis; moreover, the Hill–Swift model predicted fracture initiation better than the NADDRG model.

ACKNOWLEDGMENT

The authors would like to gratefully acknowledge Mr. M. Nezami who helped them during tests and also, provided the hydraulic press and other necessary equipments for the project.

REFERENCES

1. Zhang, S.H.; Danckert, J. Development of hydro-mechanical deep drawing. Int. J. Mech. Sci. **1999**, *40*, 1800–1807.
2. Lang, L.H.; Wang, Z.R.; Kang, D.C.; Yuan, S.J.; Zhang, S.H.; Danckert, J.; Nielsen, K.B. Hydroforming highlights: Sheet hydroforming and tube hydroforming. Journal of Materials Processing Technology **2004**, *151*, 165–177.
3. Lang, L.; Danckert, J.; Nielsen, K.B. Investigation into hydrodynamic deep drawing assisted by radial pressure Part I. Experimental observations of the forming process of aluminum alloy. J. Mat. Proc. Tech. **2004**, *148*, 119–131.
4. Lang, L.; Danckert, J.; Nielsen, K.B. Investigation into hydrodynamic deep drawing assisted by radial pressure Part II. Numerical Analysis of the drawing mechanism and the process parameters. J. Mat. Proc. Tech. **2005**, *166*, 150–161.
5. Zhang, S.H.; Jensen, M.R.; Nielsen, K.B.; Danckert, J.; Lang, L.H.; Kang, D.C. Effect of anisotropy and prebulging on hydromechanical deep drawing of mild steel cups. J. Mat. Proc. Tech. **2003**, *142*, 544–550.
6. Kandil A. An experimental study of hydroforming deep drawing. J. Mat. Proc. Tech. **2003**, *88*, 70–80.
7. Tirosh, T.; Yossifon, S.; Eshel, R.; Betzer, A.A. Hydroforming process for uniform wall thickness products. Trans. ASME. **1977**, *99*, 685–691.
8. Shima, H.; Yang, D.Y. A simple method to determine pressure curve for sheet hydroforming and experimental verification. J. Mat. Proc. Tech. **2005**, *167*, 169–177.
9. Harpell, E.T.; Workswick, M.J.; Finn, M.; Jain, M.; Martin, P. Numerical predication of the limiting draw ratio for the aluminum alloy sheet. J. Mat. Proc. Tech. **2000**, *100*, 131–141.
10. Keum, Y.T.; Lee, K.B. Sectional finite element analysis of forming processes for aluminum-alloy sheet metals. Int. J. Mech. Sci. **2000**, *42*, 1911–1933.
11. Bleck, W.; Deng, Z.; Papamantellos, K.; Oliver, Ch. A comparative study of the forming-limit diagram models for sheet steels. J. Mat. Proc. Tech. **1998**, *83*, 223–230.
12. Kawka, M.; Olejnik, L.; Rosochowski, A.; Sunaga, H.; Makinouchi, A. Simulation of wrinkling in sheet metal forming. J. Mat. Proc. Tech. **2001**, *109*, 283–289.
13. Slota, J.; Spisak, E. Comparison of the forming limit diagram (FLD) models for drawing quality of sheets. Metalurgija **2005**, *4*, 249–253.
14. Holmberg, S.; Enquist, B.; Thilderkvist, P. Evaluation of sheet metal formability by tensile tests. J. Mat. Proc. Tech. **2004**, *145*, 72–83.